report, application of "travel time" tomography is discussed. This method uses time of flight (first arrival travel times and amplitudes) to derive velocity or attenuation images.

2.2.1.1 Travel Time Tomography

Travel time tomography (Dines and Lytle, 1979) involves imaging the seismic properties from the observation of the transmitted compressional or shear first arrival energy. The relationship between the velocity field v (x,y), travel time t_i, and distance ds is given by the line integral (for a ray i):

$$t_i = \int_{R_i} \frac{ds}{v(x,y)} \qquad (1)$$

where R_i denotes the curve connecting a source receiver pair which yields the least possible travel time according to Fermat's principle. Tomography is an attempt to match calculated travel times (model responses) to the observed data by inversion of these line integrals. Initially, the region of interest is divided into a rectangular grid of constant velocity cells (j) and a discrete approximation of the line integral is assumed as:

$$t_i = \sum_j \Delta S_{ij} \cdot n_j \qquad (2)$$

where ΔS_{ij} is the distance traveled by ray i in cell j, and n_j slowness within cell j. Using a first order Taylor expansion and neglecting residual error, Equation (2) can be written in matrix form as:

$$\underline{y} = \mathbf{A}\,\underline{x} \qquad (3)$$

where the vector $\underline{y}$ is defined as the difference between computed travel times (from the model) and the observed travel times, vector $\underline{x}$ as the difference between the true and the modeled slowness, and **A** is the Jacobian matrix. In travel time tomography, Equation (3) is solved using matrix inversion techniques.

In this inversion technique, Equation (3) is commonly solved by using two series expansion approaches from geophysics: 1) matrix inversion approach (e.g. Conjugate Gradient (CG) matrix inversion technique (Nolet, 1987; Scales, 1987)); and 2) "Back-projection" inversion technique, adapted from medical tomography (e.g. Simultaneous Iterative Reconstruction Technique (SIRT)) (e.g. Herman, 1980; Ivanson, 1986).

In both techniques, the acoustic wavefield is initially propagated through a presumed theoretical model and a set of travel times are obtained by ray-tracing (forward modeling step). The travel time equations are then inverted iteratively to reduce the root mean square (RMS) error between the observed and computed travel times (inversion step). The inversion results can be used for imaging the velocity (travel time tomography) and attenuation (amplitude tomography) distribution between boreholes or access tubes.

A number of software algorithms for performing travel time tomography exist. These algorithms utilize straight or curved rays for forward model, 2-D or 3-D matrix inversion, and 2-D or 3-D graphic packages to display the results.

For accurate volumetric imaging of anomalies in concrete structures, it is critical to use a software package with the following characteristics: a) curved ray tracing or wave propagation based forward modeling; b) True 3-D matrix inversion; c)- 3-D display of data.

A "true 3-D" tomographic program inverts for the full 3-D velocity *volume* in a single step. As is shown in the next section, software packages that, for example, use 2-D inversion followed by the 3-D display of the results, do not render an adequate volumetric definition of anomalies or defects. Two-dimensional tomographic inversion produces defect images with lower resolution than 3-D inversion as imaging is done independently in 2-D planes (panels). In addition, in the next section, a critical velocity equalization Quality Control (QC) processing step is described. Velocity equalization is performed prior to the tomographic inversion for minimizing artifacts in the imaged space.

2.2.2 Tomography Pre-Processing – Velocity Equalization

Three-dimensional tomographic velocity inversion requires the critical step of velocity equalization. Velocity equalization is also important for 2-D velocity inversion. Velocity equalization involves in static shifts of zero and offset CSL logs in order to equalize background (shaft) velocity in all the test panels. Velocity equalization is necessitated due to inaccurate measurements of tube geometries in the field—such as inaccurate measurement of tube separation due to the bending of tubes at the surface. It can also be due to the "cycle skipping" (missing the right leg in picking travel times) especially in picking high angled offset logs.

Proprietary three-dimensional velocity equalization software is used which normalizes the background (shaft) velocity in three-dimensions prior to the tomographic inversion. This step is important for CSLT imaging as edge (boundary) artifacts are reduced. For true 3-D imaging, however, velocity equalization is critical; otherwise false anomalies can be created if large velocity contrasts exist between the panels.

To demonstrate the importance of velocity equalization step, 2-D and 3-D tomographic results from Amherst-NGES Shaft 1 are shown in Figure 12 before and after velocity equalization (top and bottom figures, respectively). As described in Section 5.1 in detail, this shaft was constructed in Amherst, MA with known engineered defects. In Figure 12, results using 3-D matrix inversion are shown on the left hand side and results using 2-D matrix inversion is shown on the right hand side. All CSLT images are displayed with the same velocity scale for comparison.

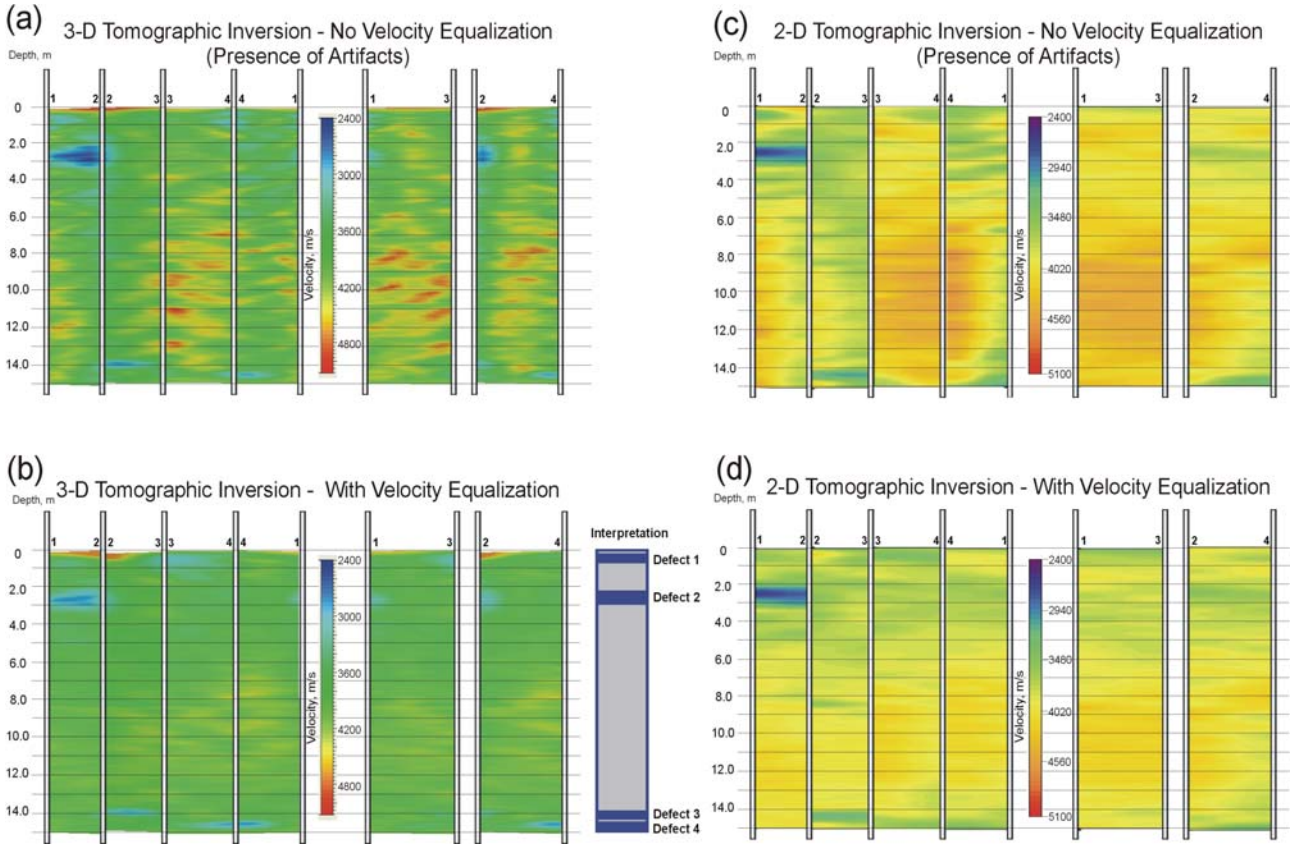

Figure 12. Schmeatic. Comparison of 2-D and 3-D Tomographic Imaging With and Without Velocity Equalization- Shaft 1, NGES, Amherst, MA.

Four defects are interpreted from the equalized 3-D tomography results of Figure 12-b and is shown to the right of this figure. For the shallow Defect 1 between the depths of 0.2-1 m, only 3-D inversion resolves this defect near Tube 3. This defect is not imaged in the 2-D inversion results of Figure 12-d. For Defect 2 between the depths of 2-3 m, both 2-D and 3-D inversions image this defect; however, 3-D inversion resolves this defect better, especially between Panels 1-3 and 2-4. For Defect 3 between the depths of 13.8-14.2 m, both 2-D and 3-D inversions image this defect between Panel 2-3. Finally, for the Defect 4 between the depths of 14.3-14.8 m, only 3-D inversion images this defect near Tube 4. Therefore, it is evident that 3-D inversion produces sharper defined images with better spatial definition.

From this figure it is also clear that artifacts are considerably reduced by the velocity equalization step. Artifacts are indicated by red and yellow colors in the 3-D inversion results shown in Figures 12-a and 12-b and by orange color in the 2-D inversion results shown in Figures 12-c and 12-d.

As a second example, results from Amherst Shaft 4 (also with known defects) are displayed in Figure 13. From this figure, three defects are interpreted from the equalized 3-D tomography results of Figure 13-b and is shown to the right of this figure. For the shallow Defect 1 (between 2.8-3.4 m depths), both the 2-D and 3-D inversions indicate this anomaly; however, 3-D

inversion resolves this defect better, especially between Panel 1-3. For Defect 2 between the depths of 5.5-6.2 m, both 2-D and 3-D inversions indicate this anomaly; however, 3-D inversion resolves this defect better. For Defect 3 between the depths of between the depths of 14.6-14.9 m, both 2-D and 3-D inversions indicate this anomaly; however, 3-D inversion resolves this defect better, especially between Panel 2-3 and 1-3. Therefore, it is evident that 3-D inversion produces sharper images with better spatial definition.

From this figure it is also evident that artifacts are considerably reduced by the velocity equalization step, especially in 3-D inversion. Artifacts are indicated by red and yellow colors in the 3-D inversion results shown in Figures 13-a and 13-b. Note, for example, that in Panel 3-4, Defects 1, 2, and 3 are masked in 3-D inversion. In 2-D inversion, notice the dramatic effect of velocity equalization in higher average velocities in Panel 2-3 (blue) before velocity equalization in Figures 13-c as compared to after velocity equalization in Figure 13-d (green).

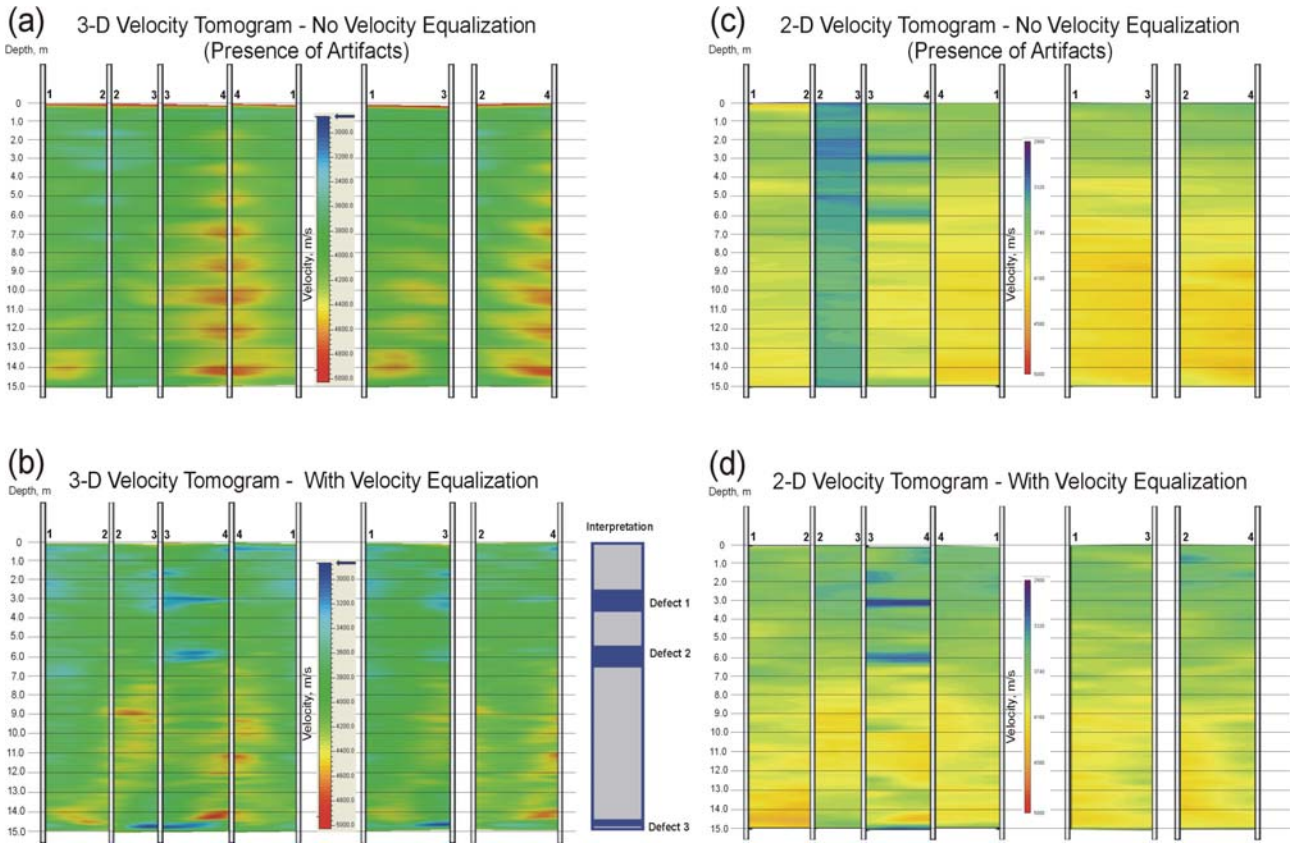

Figure 13. Schematic. Comparison of 2-D and 3-D Tomographic Imaging With and Without Velocity Equalization- Shaft 4, NGES, Amherst, MA.

Therefore, it is recommended to use velocity equalization followed by true 3-D tomographic inversion of the data in order to obtain best resolution in defining defects and in minimizing artifacts in the imaged space.

2.2.3 Tomography Modeling

Synthetic forward modeling was performed to examine the resolution and accuracy of typical CSLT acquired data. The first task addresses how well typical offset tomography field acquisition images or resolves defects. The second task addresses how well these final tomography images represent the true velocity field so that it can be correlated it to concrete strength.

2.2.3.1 CSLT Offset Tomography as an Imaging Tool

The degree tomography can image or resolve a defect depends on how completely one can surround the test volume with sources and receivers and scan it (aperture). Since a full 360º scanning is not possible, and tomography is an iterative a priori based error reduction process, a perfect image of defects can never be obtained, even under ideal modeling where perfect data picking is assumed.

To examine the effectiveness of typical CSLT field acquired data in resolving defects in a drilled shaft foundation, three synthetic models are created:

Model 1: Shaft with a Small Defect**.** As shown in the left hand side of Figure 14-a, a 2-D model is created consisting of two access tubes 1.0 m apart with a (0.4x0.5m) defect representing 2% of total area. The model consists of sound concrete at 4,000 m/s, shown in light purple, and defect at 2,000 m/s, shown in dark purple. This model is used to examine the resolving power of different combinations of CSLT field acquired offset log data.

First, the results using standard zero probe offset CSL process is shown next to the model in Figure 14-a. These images were obtained by inputting a single "zero-offset" CSL log into the tomographic imaging software. It is apparent from Figure 14-a that standard CSL horizontally smears (elongates) defects due to the lack of angular ray coverage. The zero-offset image is shown with and without ray paths superimposed.

Next, in order to systematically observe the improvement in CSLT images, the zero-offset CSL log is progressively combined with just one other offset log. These two combination logs are formed by combining 0º CSL logs with one other offset log ±11.25º, or ±22.5º, or ±45º as shown in Figures 14-b to 14-d, respectively. As expected improvement in image resolution is observed; however, the best improvement is observed by combining zero-offset logs with ±45º logs as high angled rays delineate the defect edges better.

Finally, zero offset logs were combined with two offset log of ±22.5º and ±45º in forming three combination logs in Figure 14-e and four combination logs of ±11.25º, ±22.5º, and ±45º in Figure 14-f. Obviously, the best image is formed using all four combinations of angled logs. Notice, however, that this image is not a "perfect" reconstruction of the model and has a slight velocity "shadow" which is typical of tomography images, as previously discussed. Nonetheless, the ray path diagram clearly delineates the four edges of the defect as points where rays are sharply turning (refracted) out.

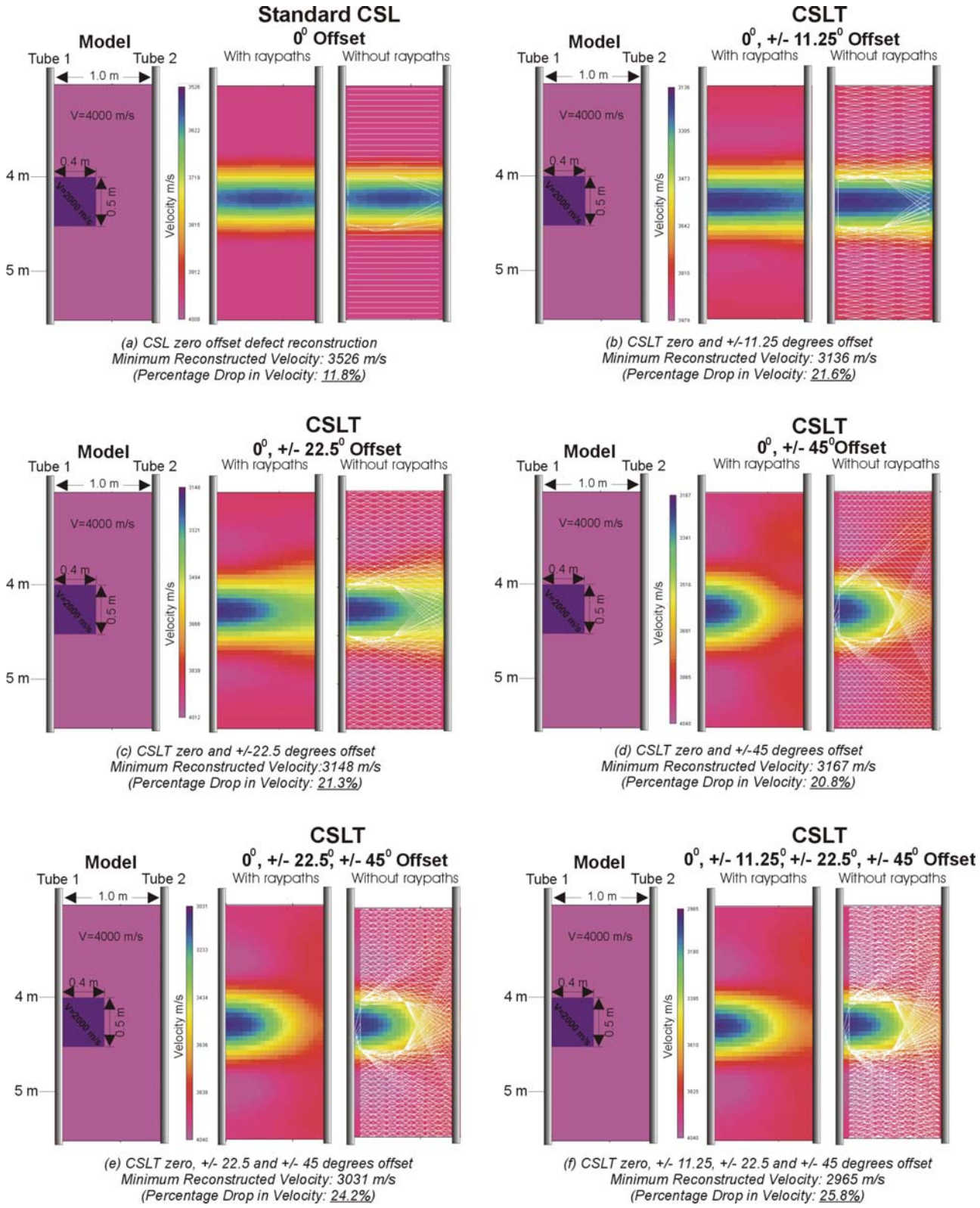

Figure 14. Schematic. Computer Based Synthetic Modeling of a Shaft with a Small Defect. Tomographic Imaging Results Comparing Standard Zero-Offset CSL Image (Top Left Hand Side) With Different Combination of Multi-Offsets CSLT Images.

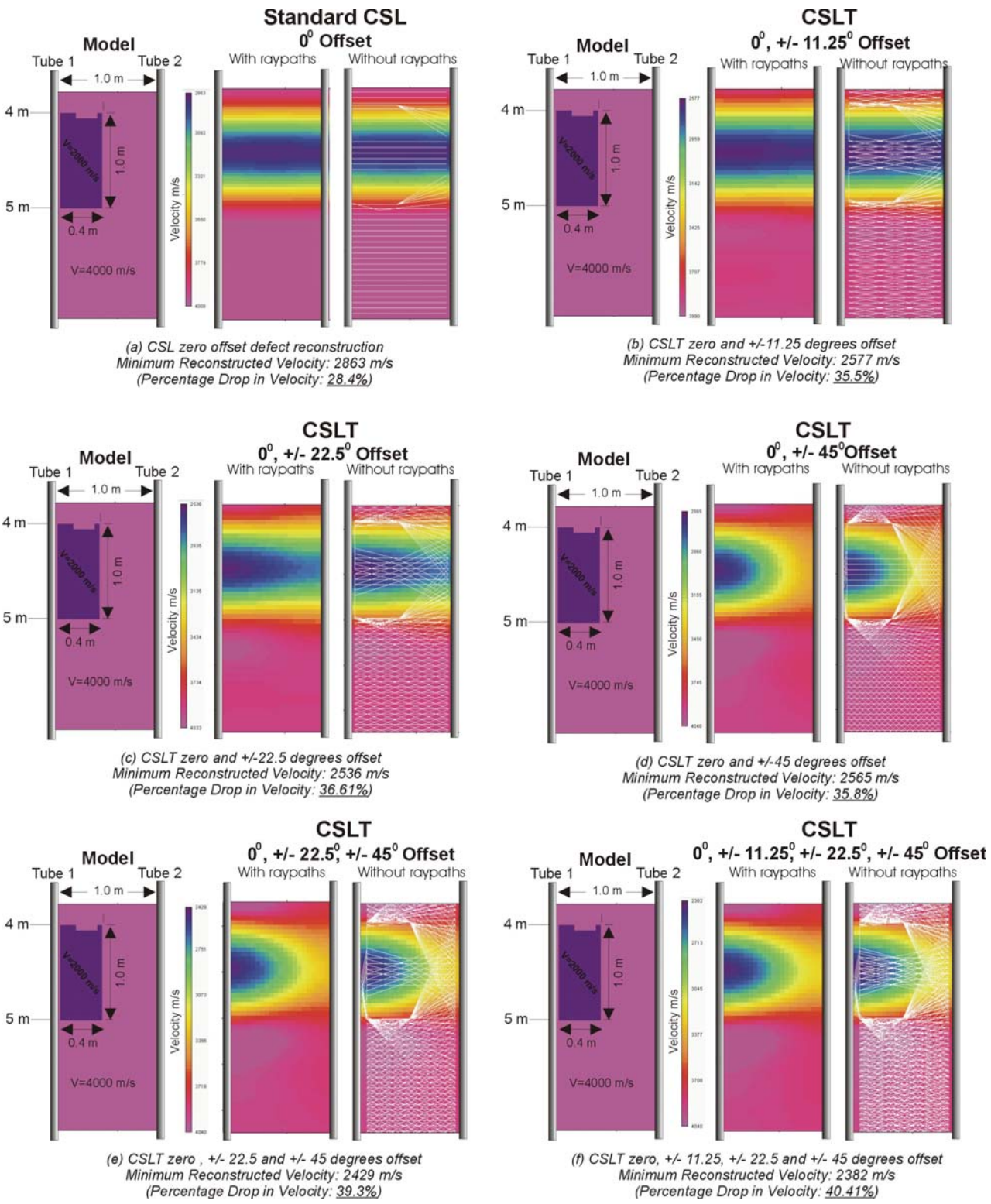

Figure 15. Schematic. Computer Based Synthetic Modeling of a Shaft with a Large Defect. Imaging Results Comparing Standard Zero-Offset CSL Image (Top Left Hand Side) With Different Combination of Multi-Offsets CSLT Images.

Surprisingly, note that just two combination of 0º and ±45º logs in Figure 14-d gave an image similar to the four combination logs of Figure 14-f, but only slightly oversized. It is apparent that even with a very coarse angular coverage (0 and 45 degree logs only), offset tomography can resolve defect boundaries sufficiently due to the fine depth sampling involved. Therefore, it is not necessarily the ray density that governs image resolution, but the presence of high angled rays. For this model of a shaft with "small" defect and the velocity contrast presented the ray paths all go around the defect with no raypath coverage (therefore, velocity reconstruction) inside.

Model 2: Shaft with Large Defect. As a second example, as shown in Figure 15, another 2-D model is created consisting of two access tubes 1.0 m apart with a defect twice as long (0.4x1m) which constitutes 4% of total 2D area. Again, similar results are obtained with 2-D CSLT using just 0º and ±45º logs in Figure 15-d producing an image similar to the four combination logs of Figure 15-f. However, due to the larger size of the defect, in all offset log combinations, few rays *are* traced inside the defect zone. Therefore, defect velocities are better reconstructed, as is described further in Section 2.2.3.2. Once again, CSLT reconstruction of offset log acquired data slightly elongates and over sizes the defect.

Model 3: Shaft with Multiple Levels of Defects. Finally, Figure 16 illustrates the results of a shaft with multiple defect levels. Multi-offset CSLT images are compared with zero-offset standard CSL "image". (This model has different velocity scale or color display than previous examples). Again, four offset CSLT acquisition provides with a good image of the defects even though multiple defect levels are present. However, CSLT exaggerate the size of anomaly, especially for smaller more elongated defects.

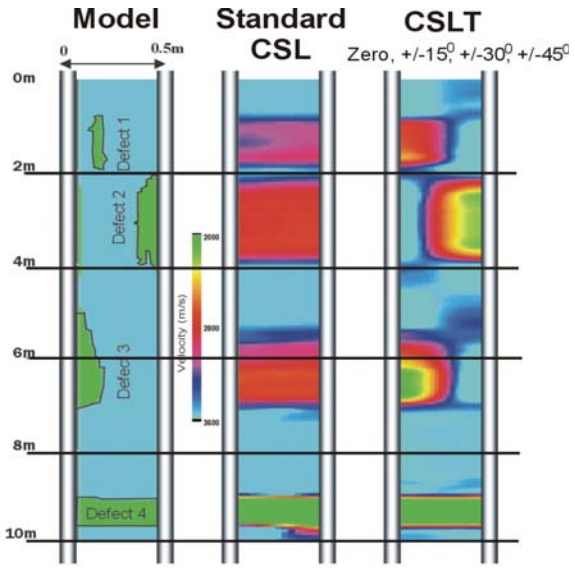

Figure 16. Schematic. Synthetic Modeling of a Shaft with Multiple Levels of Defects. Tomographic Imaging Results Comparing Standard Zero-Offset CSL Image With Multi-Offset CSLT Image.

Therefore, it is concluded that multi-offset CSLT reconstruction is a good *imaging* tool, but slightly over sizes defects.

2.2.3.2 Tomography as an Accurate Representation of the Velocity Field

To examine how well CSLT represents the velocity field (especially the defect velocity), percentage drops in minimum defect velocity as compared to the shaft velocity is presented in Figure 17. The percentage values are presented for the small and large defects in Figs. 14 and 15 with the solution (model) corresponding to 50% drop from 4,000 m/s to 2,000 m/s.

Note that tomography does not provide a perfect reconstruction of velocity field, especially for small defect or low velocity defects such as void. Larger, or higher velocity defects (low velocity contrast), provide a better reconstruction of velocity as rays travel inside the defect. Since most common defects in drilled shaft are relatively larger size with low velocity contrast, it appears the defect velocities must be reduced by about 30% for 2-D inversion and slightly less in 3-D (as described in Section 2.2.2)—even though more modeling is needed.

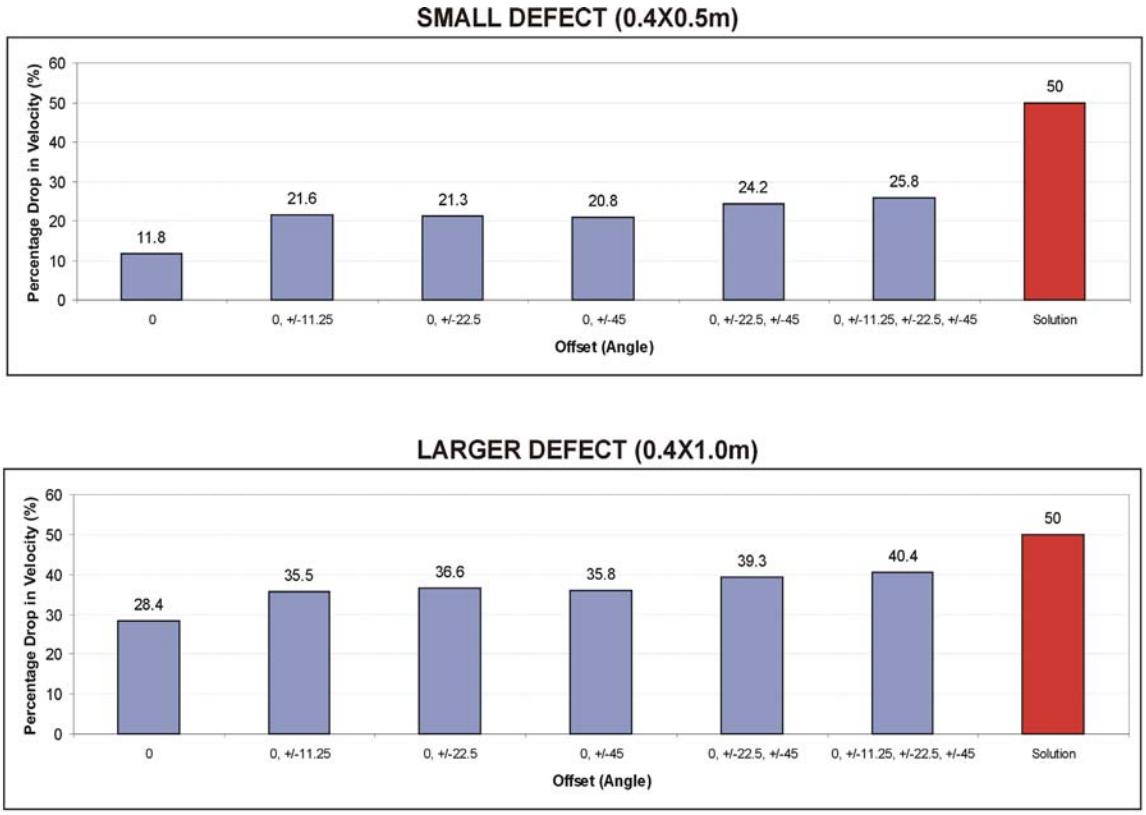

Figure 17. Schematic. Correlation between Percentages Drops in Velocity of Standard CSL Versus Number of Combination of CSLT Tomography.

In conclusion, tomography slightly over sizes and elongate defects but underestimates their velocities. Therefore, there is a compensation effect; nevertheless, a corrective factor needs to be applied to the defect velocities to accurately calibrate their values to concrete strength (for details, refer to Chapter 4).